

ISSN 1803-1269 (Print) | ISSN 1805-0476 (On-line)

Special Issue | HSM 2025

18th International Conference on High Speed Machining October 15-16, 2025, Metz, France

DOI: 10.17973/MMSJ.2025_11_2025131



HSM2025-45838

INFLUENCE OF SPATIAL ENGAGEMENT CONDITIONS ON WORKPIECE TEMPERATURE IN GRINDING OF UNIDIRECTIONAL CFRP

Alexander Brouschkin^{1*}, Ganna Shchegel¹, Carsten Möller¹, Jan Hendrik Dege¹

¹Institute of Production Management and Technology, Hamburg University of Technology, Germany

*Corresponding author; e-mail: alexander.brouschkin@tuhh.de

Abstract

Carbon Fibre Reinforced Polymers (CFRP) are favoured for their high strength to weight ratio, excellent directional mechanical and thermal properties, and the ability to be optimized in the direction of stress or heat flow. These properties make it ideal for power transmission applications. Heating of the machined surface during grinding can lead to reduced workpiece quality, particularly if the glass transition temperature of the matrix is exceeded. The selection of tool-material, process parameters and cooling strategy significantly influences heat flow from the region of tool-workpiece interaction and changes in the workpiece temperature. Machining unidirectional CFRP is challenging due to its anisotropic behaviour, resulting in different machining temperatures for identical parameters with different fibre orientations. A universal process-independent model describing the spatial engagement conditions during oblique cutting of unidirectional CFRP was used. The model introduces the spatial fibre cutting angle θ_0 and the spatial engagement angle ϕ_0 . Using this description, an experimental setup for investigating the workpiece surface temperature of CFRP for all possible engagement conditions was developed. In this paper, the machining temperature is determined for all possible spatial engagement conditions during the machining of CFRP using thermographic camera. Furthermore, the influence of the cutting material in the cases of corundum and diamond is analysed as well as the influence of the cutting speed.

Keywords:

Grinding, Carbon fibre reinforced polymers, Temperature

1 INTRODUCTION

The use of Carbon fibre reinforced polymers (CFRP) is based on their excellent strength to weight ratio. CFRP consists of carbon fibres and a polymer matrix. The fibres are anisotropic. They are responsible for transferring mechanical and thermal loads in the composite. The polymer matrix supports the fibres to resist shear forces and protects the fibres from the environment.

The behaviour of the material in the finished component is influenced by the fibre reinforcement. This also applies to its behaviour during mechanical processing in production. As such, it determines the dominant directions of heat flow and the resulting temperature distribution during machining of composite components [Mehnen 2019].

This is particularly true for trimming, which is necessary to achieve accurate geometric contours and high surface quality in finished parts [Kerigan 2016, Seo 2024]. It has been well documented [Wang 2016, Delahaihue 2017] that during typical machining operations, surface temperatures can exceed the glass transition temperature $T_{\rm g}$ and even the thermal degradation temperature of the epoxy resin. The consequence of exceeding the glass transition temperature $T_{\rm g}$ is a severe degradation of the mechanical properties of the matrix and its ability to support the fibres. The loss of fibre support leads to poor surface integrity and delamination, which can act as stress concentrators and initiate crack propagation under load [Mullier 2014, Prakash 14].

Tools with geometrically defined cutting edges, such as end mills [Wan16, Liu 2024a] and drills [Liu 2024b], are used for contouring and drilling respectively. Grinding tools with geometrically indeterminate cutting edges are used both for surface machining and for contour machining of component contours [Soo 2012].

Different cutting materials have an effect on workpiece temperature. Sheikh-Ahmad et al. calculated that the temperature of a surface machined with a polycrystalline diamond cutter should be higher than that of a surface machined with a TiAIN-coated peripheral endmill. The temperature can be measured using a set of thermocouples placed at a defined distance from the machining process. Another method is to use a thermographic camera to film the area adjacent to the machined surface. [Sheikh-Ahmad 2019]

Hintze et al. introduce a universal, process-independent model to describe the engagement conditions for oblique cutting of unidirectional CFRP. This model allows the description of all arbitrary engagement conditions with the spatial fibre cutting angle θ_0 and the spatial engagement angle φ_0 . [Hintze 2022]

This paper investigates the machining temperature during peripheral grinding of CFRP under arbitrary spatial engagement conditions. In addition, the influence of the cutting speed v_c and the cutting materials corundum and diamond on the cutting temperature is evaluated.



ISSN 1803-1269 (Print) | ISSN 1805-0476 (On-line)

Special Issue | HSM 2025

18th International Conference on High Speed Machining

DOI: 10.17973/MMSJ.2025_11_2025131

October 15-16, 2025, Metz, France



Nomenclature

Nomenciature		
CFRP	Carbon fibre reinforced polymer	
Cor.	Corundum	
Dia.	Diamond	
$e_{ },e_{\perp 1},e_{\perp 2}$	Coordinate system of the CFRP laminate	
e_r, e_s, e_o	Coordinate system of the cutting tool	
P_{S}	Cutting plane	
P_f	Tool-reference plane	
P_o	Tool-orthogonal plane	
θ	Fibre cutting angel [°]	
χ, ξ	Reference angles [°]	
θ_0	Spatial fibre cutting angle [°]	
$arphi_0$	Spatial fibre engagement angle [°]	
ϕ	Engagement angle [°]	
ρ	CFRP sample tilt angle [°]	
Vc	Cutting speed [m/s]	
Vf	Feed velocity [mm/min]	
f	Feed rate [mm/rev]	
n	Spindle speed [rpm]	
a_e	width of cut [mm]	
a_p	depth of cut [mm]	
h	Undeformed chip thickness [mm]	
I _f	grinding path [mm]	
t_b , b_b , l_b	Dimensions of the CFRP block [mm]	
D	Grinding wheel diameter [mm]	
b	Grinding wheel width [mm]	
Gr	Grit size [mesh]	
G	Grain size [µm]	
S	Structure of the grinding wheel	
ϕ	Engagement angle [°]	
T_{max}	maximum Temperature [°C]	
ϵ_m	emissions coefficient	
1		

2 PROCESS-INDEPENDENT DESCRIPTION OF FIBRE ENGAGEMENT CONDITIONS

Hintze et al. [Hintze 2022] introduce a process-independent description of the spatial engagement conditions during the oblique cut of CFRP with reference angles. Due to a transformation of the workpiece coordinate system $\{e_{\parallel}, e_{\perp 1}, e_{\perp 2}\}$ into the tool coordinate system $\{e_r, e_s, e_o\}$ (Fig. 1) all spatial engagement can be described with the reference angles θ , χ , ξ and the inclination angle λ_s . Because of the orthotropy of CFRP, Hintze et al. [Hintze 2022] introduced the spatial engagement angles θ_0 and φ_0 . The spatial fibre cutting angle θ_0 is between the vectors, $\mathbf{e_s}$ and $\mathbf{e}_{||}$ and the spatial engagement angle φ_0 is between the

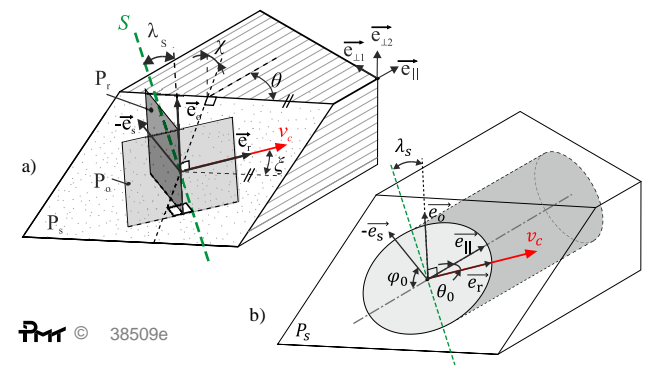


Fig. 1: a) Workpiece coordinate system and the tool coordinate system with the reference angles, b) spatial engagement angles

vectors $\mathbf{e_r}$ and $\mathbf{e_{||}}$, as shown in Fig. 1a. With the equations (1-3) the angles θ_0 and φ_0 can be calculated:

$$\begin{pmatrix} \mathbf{e}_{\parallel} \\ \mathbf{e}_{\perp 1} \\ \mathbf{e}_{\perp 2} \end{pmatrix} = \begin{bmatrix} \cos \theta & \sin \theta & 0 \\ -\sin \theta & \cos \theta & 0 \\ 0 & 0 & 1 \end{bmatrix} \cdot \begin{bmatrix} 1 & 0 & 0 \\ 0 & \cos \chi & \sin \chi \\ 0 & \sin \chi & \cos \chi \end{bmatrix} \cdot \begin{bmatrix} \cos \xi & 0 & -\sin \xi \\ 0 & 1 & 0 \\ \sin \xi & 0 & \cos \xi \end{bmatrix} \cdot \begin{pmatrix} \mathbf{e}_{\mathbf{r}} \\ \mathbf{e}_{\mathbf{s}} \\ \mathbf{e}_{\mathbf{o}} \end{pmatrix}$$
(1)

$$\cos(\theta_0) = \langle \mathbf{e_r}, \mathbf{e_{||}} \rangle \tag{2}$$

$$\cos(\varphi_0) = \langle \mathbf{e}_{\mathbf{s}}, \mathbf{e}_{||} \rangle \tag{3}$$

Considering that the spatial fibre cutting angle θ_0 lies in the cutting plane P_s and the spatial fibre engagement angle φ_0 is determined using a vector orthogonal to the cutting plane, the following equations results:

$$0 \le \varphi_0 \le 90^{\circ} \tag{4}$$

$$90^{\circ} - \varphi_0 \le \theta_0 \le 90^{\circ} + \varphi_0 \tag{5}$$

3 EXPERIMENTAL SETUP

The experiments are carried out using the experimental setup shown in Fig. 2. A unidirectional CFRP specimen (HexPly 6367, HTS-(12K)) is clamped to a dynamometer (Kistler 9257B). The glass transition temperature $T_g \approx$ 200°C of the used CFRP was determined using Temperature-Modulated Differential Scanning Calorimetry [Stark 2013]. Grinding wheels with an outer diameter of D =200 mm and a width of b = 20 mm are used. Two different cutting materials are used: Corundum with a ceramic bond, a grit size of Gr = 46 mesh ($G = 301 \mu m$) and a structure of S = 11 and single-layer electroplated diamond with a grain size of $G = 301 \mu m$. The experiments are carried out with a constant width of cut $a_e = 0.1$ mm, a constant feed rate f =0.15 mm/rev and without coolant.

Tab. 1: Variation of spatial engagement conditions

Tilt ρ [°]	Fibre cutting angle θ [°]
0	0, 30, 45, 60, 90, 120, 135, 150, 180
30	0, 30, 45, 60, 120, 135, 150, 180
60	0, 30, 45, 60, 120, 135, 150, 180
90	0, 30, 45, 60, 90, 120, 135, 150, 180



ISSN 1803-1269 (Print) | ISSN 1805-0476 (On-line)

Special Issue | HSM 2025

18th International Conference on High Speed Machining

October 15-16, 2025, Metz, France DOI: 10.17973/MMSJ.2025_11_2025131



Grinding wheel

Thermographic camera

CFRP - sample

Dynamometer

Dynamometer

A - A

A

A

A

A

A

A

A

A

A

Fig. 2: Experimental setup

The cutting speed v_c = 10|25|40 m/s is varied resulting in different feed velocities v_f = 143|358|573 mm/min.

In a machining operation prior to the examination, a block with the dimensions t_b = 4.0 mm, b_b = 6.5 mm and l_b = 6.0 mm is prepared at the tip of the sample in order to avoid interference with the disc face during the main examination. The square cross-sectional area is always aligned parallel to the feed direction. Different spatial engagement conditions are realised by varying the fibre cutting angle θ and the CFRP-sample tilt angle ρ (Tab. 1). As a result of the large disc diameter and the low material thickness, the engagement angle can be assumed to be $\phi \approx 90^\circ$ over the entire engagement range. The following applies to the calculation of the spatial engagement conditions:

$$\chi = 0^{\circ}; \xi = \rho \tag{6}$$

$$\theta_0 = \arccos[\cos(\theta) \cdot \cos(\xi)]$$
 (7)

$$\varphi_0 = \arccos[\sin(\theta)] \tag{8}$$

Regarding equations (4) and (5) ρ = 0° ... 90° and θ = 0° ... 180° is sufficient to cover all possible engagement conditions. The position of the measurement points in the θ_0, φ_0 -plane is shown in (Fig. 3).

To generate a measurement comparable to that of a long cutting length despite the short cutting length, the grinding wheel moves back and forth five times during the test for a total cutting length $I_f = 20$ mm without lingering at the reversal points. The centre plane of the prepared block is positioned directly in the middle of the cutting path. Each time the direction is changed, the width of the cut a_e is adjusted. This results in ten repetitions of the grinding process. The resulting up and down grinding is evaluated independently.

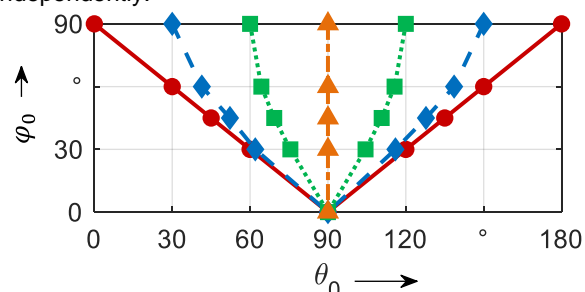
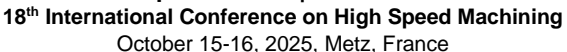


Fig. 3: Measurements in θ_0 - φ_0 -plane



ISSN 1803-1269 (Print) | ISSN 1805-0476 (On-line)

Special Issue | HSM 2025



DOI: 10.17973/MMSJ.2025_11_2025131



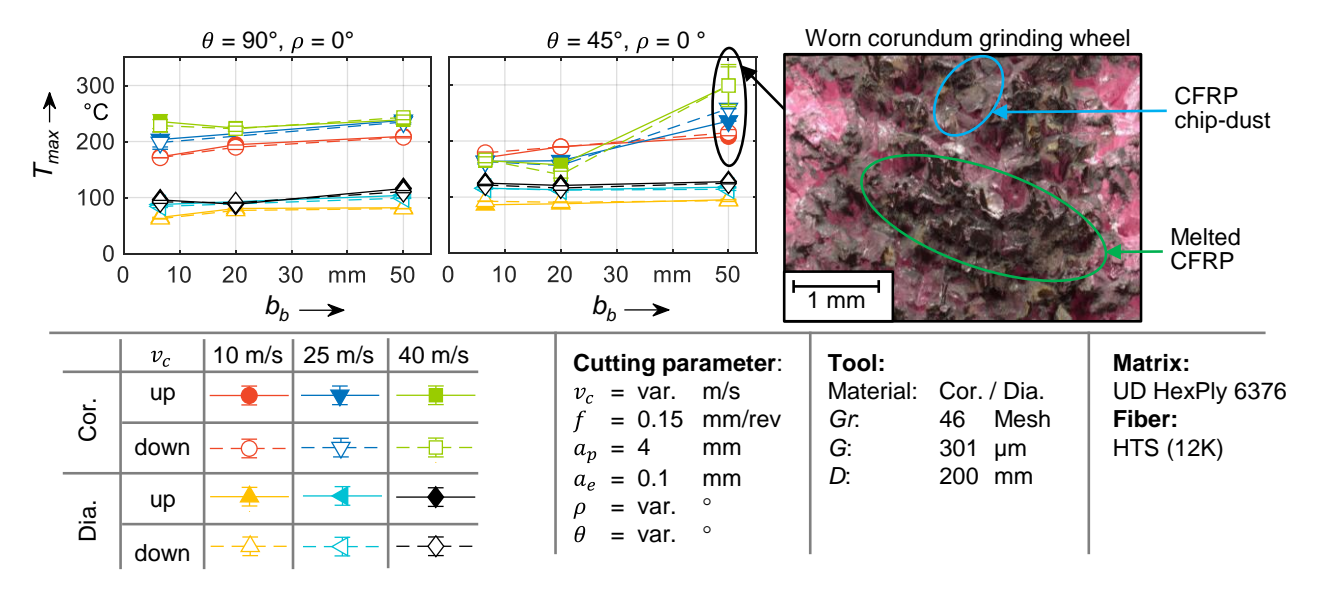


Fig. 4: Experimental results on the influence of cutting length bb

As the corundum wheel showed significant wear, for each CFRP-sample inclination angle ρ , the corundum wheel was redressed. Because the diamond wheel showed no signs of wear and a redressing of a single-layer electroplated diamond grinding wheel is not possible, the diamond wheel wasn't redressed.

The temperature is measured using a thermographic camera (Micro-Epsilon thermolMAGER TIM 640 VGA) with an image section measuring 640 x 120 pixels and a sampling rate of 125 Hz. A standard lens with an angle of view of 33° and a focal length of 18.7 mm was used. The camera was positioned 750 mm from the object being measured. A standard temperature range of 0-250 °C was selected. If the temperature exceeded 250°C, a second run was performed within the temperature range of 150-900°C. To determine the emissions coefficient ϵ_m of the CFRP, separate tests were conducted. To achieve this, a steady temperature state was reached in a CFRP panel with installed thermocouples using an external heater. The emissivity value of ϵ_m = 0.95 was adopted for the temperature range of 30 °C-180 °C to ensure that the average temperature error remained below 3 °C. This corresponds to reported values in the literature for CFRP [Adibekyan 2019]. Higher temperatures were not tested in order to prevent thermal degradation of the sample, as the glass transition temperature T_g is 250 °C for this CFRP. According to the literature [Bentz 2010], the overall temperature dependence of material emissivity shows a tendency to lower emissivity values at high temperatures. Therefore, assuming a constant emissivity value higher temperatures could lead to an underestimation of the actual material temperature when measured by an infrared

The surface area of the prepared block which is parallel to the tool orthogonal plane from the top direction of the view A-A in Fig. 2, is used for the measurement. When analysing the temperature, it is assumed that the highest temperature T_{max} on the workpiece is the immediate grinding temperature, so that only the maximum temperature at one point in time is measured. The highest temperature measured during the grinding process is recorded. Of the

ten cuts per sample, the first two cuts are ignored. The remaining eight are analysed individually in the categories: up and down grinding.

4 EXPERIMENTAL RESULTS

4.1 Influence of the cutting length

In order to check whether the short machining length b_b = 6.5 mm is sufficient for generating a realistic cutting temperature T_{max} , tests are carried out under ρ = 0° and θ = 45° | 90° with machining lengths b_b = 6.5 | 20.0 | 50.0 mm.

Fig. 4 shows the evolution of the cutting temperature T_{max} over the cutting length b_b . In general, corundum has a higher cutting temperatures T_{max} than diamond. The short cutting length $b_b = 6.5$ mm results in a cutting temperature difference $\Delta T \approx 30^{\circ} \text{C}$ lower than for longer cutting lengths $b_b \gg 6.5$ mm. The grinding wheel reaches a critical wear state leading to excessive temperatures and decomposition of the polymer matrix of the CFRP at $\theta = 45^{\circ}$ and $b_b = 50$ mm. This can be seen by the black deposits on the grinding wheel (Fig. 4). The grey deposits in this image are CFRP chips. The wear condition makes the study of corundum as a cutting material challenging and difficult to reproduce.

There is no significant difference between up-cutting and down-cutting in this investigation. The cutting temperature T_{max} increases with increasing cutting speed. The increase is degressive, as a higher temperature increase was observed between v_c = 10 m/s and v_c = 25 m/s than at v_c = 25 and v_c = 40 m/s.

This study shows that for certain spatial engagement conditions, the results obtained can be considered representative even with a difference $\Delta T = 30^{\circ}\text{C}$ for large cutting lengths.

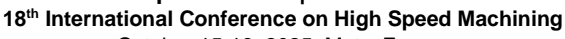
4.2 Influence of the spatial engagement conditions

Fig. 5 shows how the fibre cutting angle, θ , affects the measured cutting temperature T_{max} at different CFRP-sample tilt angles and cutting speeds v_c . Corundum



ISSN 1803-1269 (Print) | ISSN 1805-0476 (On-line)

Special Issue | HSM 2025







DOI: 10.17973/MMSJ.2025_11_2025131

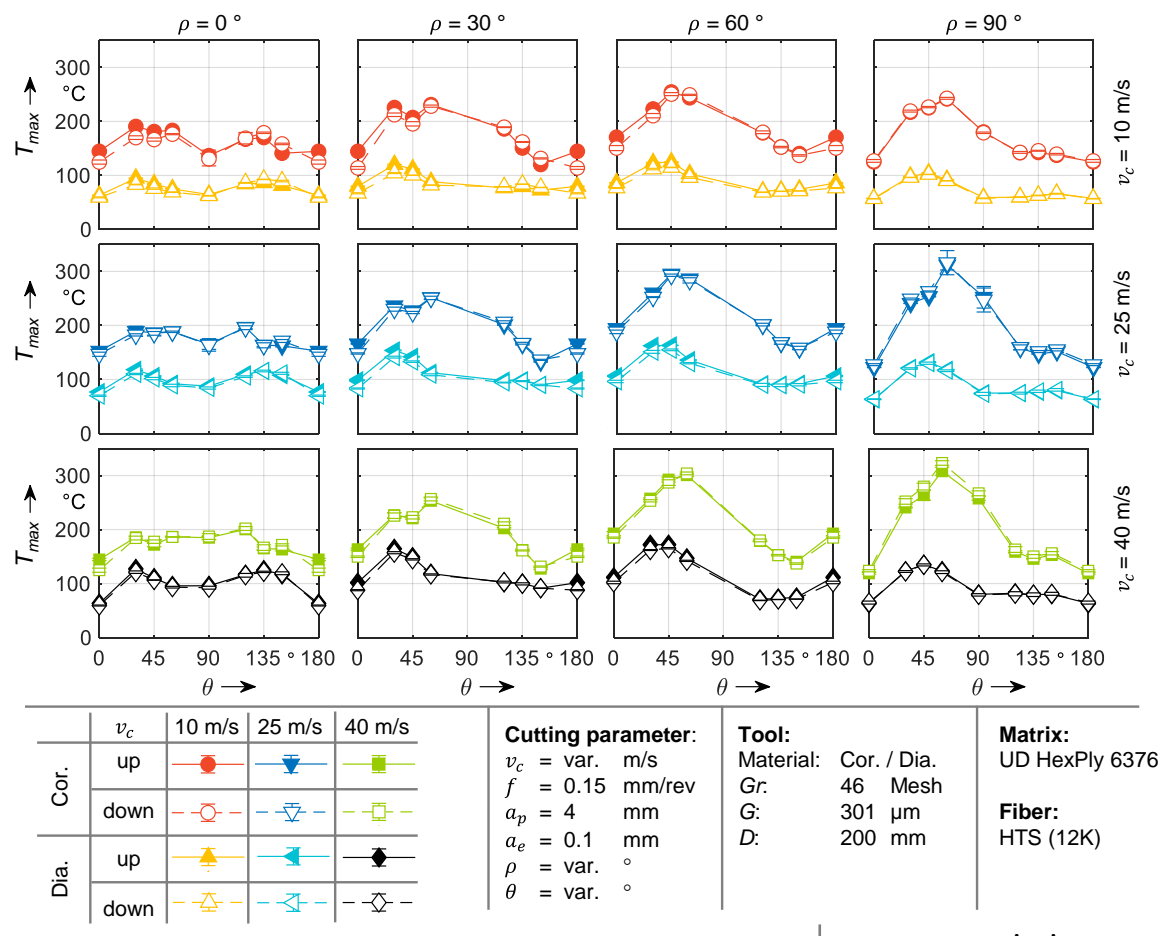


Fig. 5: Influence of θ , ρ and cutting speed v_c

generally generates significantly higher cutting temperatures T_{max} than diamond. This is due to a poorer thermal conductivity of corundum and its ceramic bond than diamond with a metallic bond on a steel base body. Consequently, the corundum tool is less effective at dissipating the heat generated during grinding. Additionally, corundum's lower hardness leads to faster wear compared to diamond. This results in increased friction and heat generation due to the impact of blunt grains.

Similar to Fig. 4, Fig. 5 shows that the cutting temperature T_{max} increases with increasing cutting speed. However, the increase is again degressive; a higher temperature increase was observed between v_c = 10 m/s and v_c = 25 m/s than between v_c = 25 m/s and v_c = 40 m/s.

The cutting temperature T_{max} on the surface is greatly affected by the fibre cutting angle θ and the tilt angle of the CFRP sample ρ . This is due to the two components of the CFRP having different thermal conductivities. Carbon fibre has high thermal conductivity, while the polymeric matrix has low thermal conductivity. Consequently, heat spreads faster in the fibre direction than across it, causing dependence on the fibre cutting angle.

At ρ = 0° and v_c = 10 m/s, the influence of the up-cut and down-cut is clearly recognizable. For fibre cutting angles θ < 90°, higher cutting temperatures T_{max} are generated by up-cutting than by down-cutting. For angles θ > 90°, however, the trend is reversed, with higher cutting

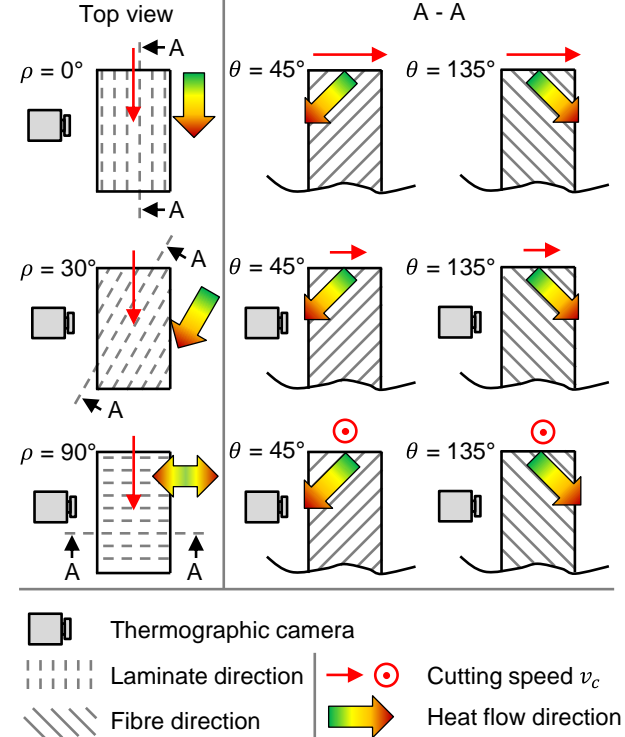
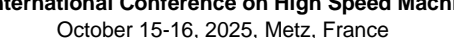


Fig. 6: Schematic view of heat flux



ISSN 1803-1269 (Print) | ISSN 1805-0476 (On-line)

Special Issue | HSM 2025 18th International Conference on High Speed Machining



DOI: 10.17973/MMSJ.2025_11_2025131



temperatures T_{max} generated by down-cutting. This behaviour remains consistent for all CFRP sample tilt angles ρ <90°. At ρ = 90°, the cutting temperatures T_{max} are the same for both up- and down-cutting. In an up-cut at θ < 90°, heat travels along the fibre with the feed movement (against the cutting speed direction). Heat accumulates at the edge of the sample, leading to higher temperatures T_{max} than in the opposite feed direction, where no heat accumulates. Heat also accumulates in the down-cut mode at fibre cutting angles of $\theta > 90^{\circ}$ and generates higher temperatures than in the up-cut mode within the same range of fibre cutting angles.

The cutting temperature T_{max} measured at the surface increases with the tilt angle of the CFRP, as does the influence of the fibre cutting angle, which varies depending on the tilt angle of the CFRP sample. In general, when considering the influence of the fibre cutting angle, it is important to distinguish between the ranges of θ < 90° and $\theta > 90^{\circ}$.

At $\rho = 0^{\circ}$, the fibre cutting angle shows almost symmetrical behaviour to θ = 90°. The lowest cutting temperature T_{max} occurs at $\theta = 0^{\circ}$ or 180°, while the maximum temperature occurs at $\theta \approx 50^{\circ}$ or 130°.

For $\rho = 30^{\circ}...90^{\circ}$, the two fibre cutting angle ranges differ. The highest cutting temperatures T_{max} occur at $\theta < 90^{\circ}$, whereas they are low at $\theta > 90^{\circ}$ and decrease as θ increases.

Fig. 6 shows an explanatory approach. Here, it is assumed that the same amount of thermal energy is transferred to the workpiece for each engagement condition.

At $\rho = 0^{\circ}$, heat flows parallel to the considered surface. This is heated indirectly by the fibres, resulting in relatively low cutting temperatures T_{max} . Because the thermal conductivity of CFRP is higher than that of air, heat builds up at the edge of the sample along the feed direction. The fibre cutting angle θ influences the amount of heat that accumulates at the samples edge. Comparable conditions symmetrical to θ = 90° are the result.

Fig. 6 illustrates that with increasing CFRP-sample tilt angle ρ more laminate planes end at the surface at which the temperature is measured. Because the fibres have a significantly higher thermal conductivity than the polymer matrix, heat flows much better within the laminate planes than across them. This leads to an increase of maximum temperatures with increasing CFRP-sample tilt angle ρ .

Because of the laminate orientation, when θ < 90°, more heat flows to the surface at which the temperature is measured as ρ increases. At $\theta > 90^{\circ}$, however, the heat flows away from the surface, resulting in lower cutting temperatures T_{max} being measured.

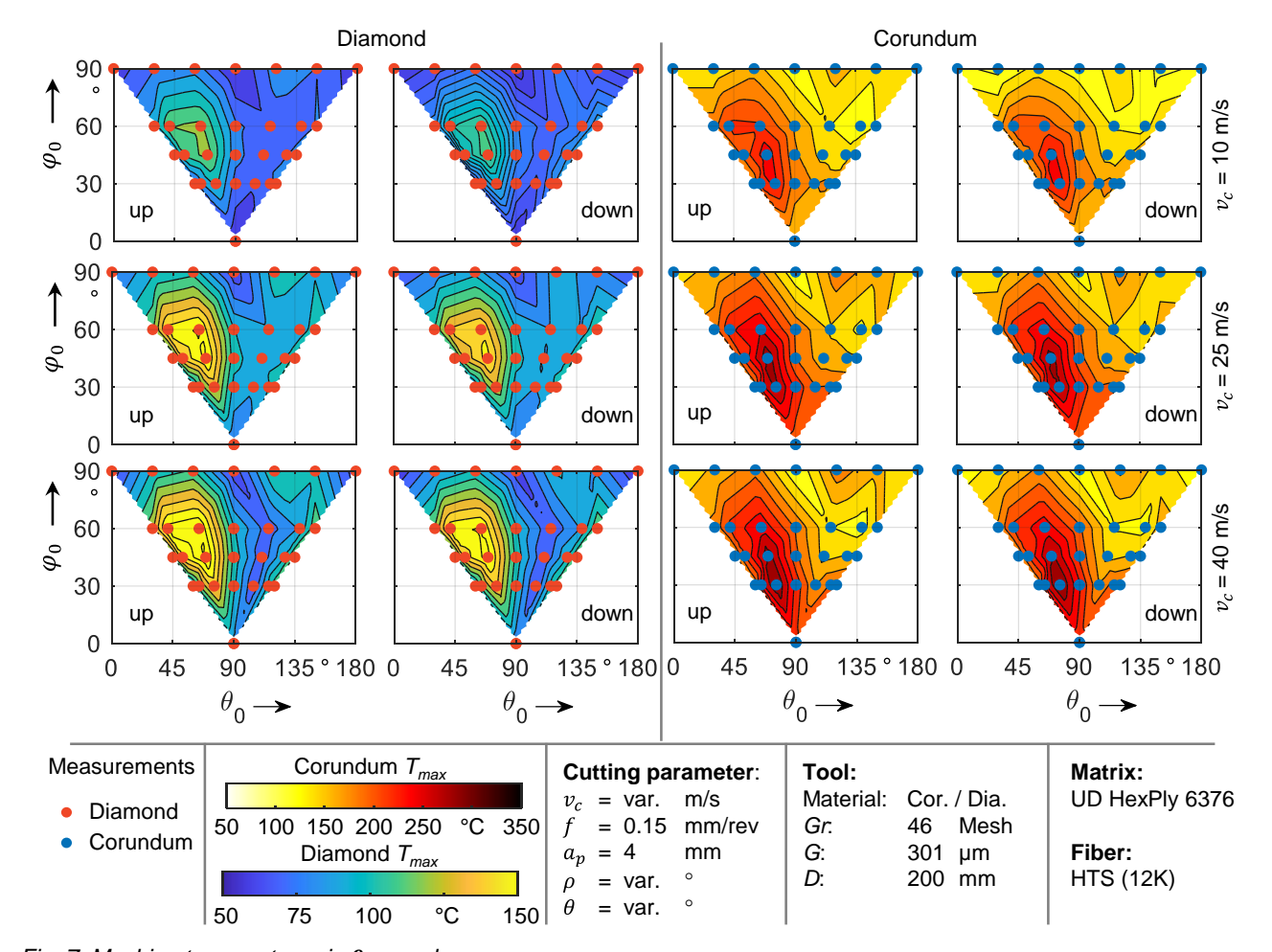


Fig. 7: Maching temperatures in θ_0 - φ_0 -plane



ISSN 1803-1269 (Print) | ISSN 1805-0476 (On-line)

Special Issue | HSM 2025

18th International Conference on High Speed Machining October 15-16, 2025, Metz, France

DOI: 10.17973/MMSJ.2025_11_2025131



According to equations (7) and (8), the same spatial engagement conditions $\theta_0, \ \varphi_0$ occur for CFRP sample tilt angle $\rho = 90^{\circ}$, but different cutting temperatures T_{max} , are measured. This demonstrates that the orientation of the measuring surface relative to the fibre direction affects the measured temperature, even when the spatial engagement conditions are the same. Therefore, to be able to compare machining temperatures, it is necessary to consider not only the spatial engagement conditions, but also the position and orientation of the measuring surface.

To ensure that the mechanical properties of the CFRP are not reduced, the glass transition temperature must not be exceeded during processing. According to Stark et al., the glass transition temperature of the CFRP used (HexPly 6367, HTS-(12K)) is approximately $T_g \approx 200^{\circ}\text{C}$ when sufficient curing time is allowed. The results presented show that machining with diamond is possible in all engagement conditions, as the machining temperature T_{max} does not exceed 200 °C. Machining with corundum, however, is problematic in many cases as 200 °C is clearly exceeded. Deposits on the grinding wheel (Fig. 4) even indicate matrix decomposition during the process. Therefore, coolant should always be used to ensure the safe use of corundum when grinding CFRP.

Fig. 7 shows the cutting temperatures T_{max} in the θ_0 - φ_0 plane. According to Equations (5) and (6), all possible engagement conditions form a triangle in the θ_0 - φ_0 -plane. In the case of $\rho = 90^{\circ}$, some engagement conditions occur twice. In this case the average temperature of the measurements is shown. This plot corresponds to that in Fig. 5. High temperatures occur within the range 15° < θ_0 < 90° and 15° < φ_0 < 75°. Low temperatures occur in the range $90^{\circ} < \theta_0 < 180^{\circ}$ and $0^{\circ} < \varphi_0 < 90^{\circ}$. In comparison with the force measurement results obtained using a defined cutting edge [Brouschkin 2024], the areas of high temperature coincide with those of low machining force. High temperatures lead to a reduction in the mechanical properties of the polymer matrix, which can explain the low cutting forces. However, the position of the surface at which the cutting temperature T_{max} is measured plays a significant role in the temperature measurement, meaning no general quantitative statements can be made about the temperature in the CFRP.

5 SUMMARY

This publication investigated the cutting temperatures T_{max} during the grinding of CFRP in all possible spatial engagement conditions, for two different cutting materials: corundum and diamond. The cutting temperature T_{max} was recorded using a thermal camera on a surface that was parallel to the tools orthogonal plane, to the right of the direction of cutting speed v_c and directly below the cutting plane. The following statements summarise how the cutting temperatures T_{max} behave depending on the spatial engagement conditions:

Cutting with corundum results in hiah temperatures T_{max} that often exceed the glass transition temperature T_g of the used CFRP. Cooling is therefore very important when using corundum.

- The diamond-cutting material results in cutting temperatures T_{max} that do not exceed the glass transition temperature $T_g = 200^{\circ}\text{C}$ of the used
- The cutting temperature T_{max} determined for short grinding lengths $b_b = 6.5 \text{ mm}$ are comparable to those for long grinding lengths with a difference $\Delta T = 30^{\circ}C$
- As the CFRP sample tilt angle ρ increases, the cutting temperature T_{max} increases within the range θ < 90° and decreases within the range θ > 90°. This is due to the different thermal conductivities of the fibres and the plastic matrix, and therefore the better heat flux along the fibres.
- The cutting temperature T_{max} shows a degressive dependence on cutting speed v_c .
- The position at which the cutting temperature T_{max} is optically measured has a significant influence on the result. Therefore, is not possible to make a statement about the temperature distribution within the sample.

Further investigations are planned to determine the cutting temperature when using cooling. Furthermore, future research will focus on developing a model for predicting cutting temperatures on other surfaces and within the sample.

6 ACKNOWLEDGEMENTS

The authors gratefully acknowledge the financial support of the Federal Ministry for Economic Affairs and Energy (Bundesministerium für Wirtschaft und Energie, BMWE) within the research project SPOTLIGHT, project number 03LB2061.

7 REFERENCES

[Adibekyan 2019]: Adibekyan A., Kononogova E., Monte C., Hollandt J.: Review of PTB measurements on emissivity, reflectivity and transmissivity of semitransparent fiberreinforced plastic composites, Int J Thermophys, 40 (2019), 10.1007/s10765-019-2498-0

[Bentz 2010]: Bentz D.P., Fire resistive materials: thermal barriers between fires and structures, Thermal conductivity 30/thermal expansion 18, NIST (2010), pp. 1-12, https://tsapps.nist.gov/publication/get_pdf.cfm?pub_id=90

[Brouschkin 2024]: Brouschkin, A., Hintze, W., Dege, J.H., Influence of spatial engagement angles on machining forces and surface roughness in turning of unidirectional CFRP. CIRP journal of manufacturing science and technology 2024, 51: 201-212, doi: 10.15480/882.9602

[Delahaihue 2017]: Delahaigue J, Chatelain J-F, Lebrun G. Influence of cutting temperature on the tensile strength of a carbon fiber-reinforced polymer. Fibers 2017;5: 46. doi: 10.3390/fib5040046.

[Hintze 2022]: Hintze, W.; Brouschkin, A.; Köttner, L.; Bluehm, M., Model Based Prediction of Force and Roughness Extrema Inherent in Machining of Fibre Reinforced Plastics Using Data Merging. Proceedings of the 12th Congress of the German Academic Association for



ISSN 1803-1269 (Print) | ISSN 1805-0476 (On-line)

Special Issue | HSM 2025

18th International Conference on High Speed Machining

October 15-16, 2025, Metz, France DOI: 10.17973/MMSJ.2025_11_2025131



Production Technology (WGP), University of Stuttgart, October 2022, Springer Verlag Berlin, doi: 10.1007/978-3-031-18318-8_5

[Kerigan 2016]: Kerrigan K, O'Donnell GE. On the relationship between cutting temperature and workpiece polymer degradation during CFRP edge trimming. Proc CIRP 2016;55: 170–5, doi: 10.1016/j.procir.2016.08.041.

[Liu 2024a]: Liu L, Qu D, Wang J, Zhang J, Cao H, Dong X. Thermal-field analytical modeling of machined surface layer in high-speed-dry milling UD-CF/PEEK considering thermal anisotropy and nonlinear thermal conductivity. Compos Appl Sci Manuf 2024;176: 10786. doi: 10.1016/j.compositesa.2023.107864.

[Liu 2024b]: Liu Y, Pan Z, Zhang H, Jing X, Zhou H, Chen Y. Thermal-mechanical coupling indrilling high-performance CFRP: scale-span modeling and experimental validation. Compos Struct 2024;331: 117903. doi: 10.1016/j.compstruct.2024.117903 j

[Mehnen 2019] Mehnen J, Hintze W, Koettner L, Von Wenserski R. Temperature field due to a moving heat source in machining orthotropic composites with arbitrary fiber orientation. Proc CIRP 2019;85: 2–7, doi: 10.1016/j.procir.2019.09.019.

[Mullier 2014]: Mullier G, Chatelain JF. Influence of thermal damage on the mechanical strength of trimmed CFRP. Int J Mech Mechatron Eng 2014;9: 1559–66, doi: 10.5281/zenodo.1109525.

[Prakash 14]: Prakash R, Krishnaraj V, Tarun GS, Vijayagopal M, Kumar GD. Experimental study on temperature effect and tool wear on edge trimming of carbon fiber reinforced plastics. J Appl Mech Mater 2014;592–594: 333–8,: doi: 10.4028/www.scientific.net/AMM.592-594.333.

[Seo 2024]: Seo J, Kim DC, Park H, Kang YS, Park HW. Advancements and challenges in the carbon fiber-reinforced polymer (CFRP) trimming process. Int J Precis Eng Manuf-Green Tech 2024;11: 1341–60. doi: 10.1007/s40684-023-00552-1.

[Soo 2012]: Soo, S. L., Shyha, I. S., Barnett, T., Aspinwall, D. K., Sim, W.-M., Grinding performance and workpiece integrity when superabrasive edge routing carbon fibre reinforced plastic (CFRP) composites. CIRP Annals, 2012, 61: 295–298., doi: 10.1016/j.cirp.2012.03.042

[Sheikh-Ahmad 2019]: Sheikh-Ahmad JY, Almaskari F, Hafeez F. Thermal aspects in machining CFRPs: Effect of cutter type and cutting parameters. Int J Adv Manuf Technol 2019;100: 2569–82, doi: 10.1007/s00170-018-2881-1.

[Stark 2013]: Stark W., Jaunich M., McHugh J.: Cure state detection for pre-cured carbon-fibre epoxy prepreg (CFC) using Temperature-Modulated Differential Scanning Calorimetry (TMDSC), Polymer Testing, 2013, 32: 1261-1272, doi: 10.1016/j.polymertesting.2013.07.007

[Wang 2016]: Wang H, Sun J, Li J, Lu L, Li N. Evaluation of cutting force and cutting temperature in milling carbon fiber-reinforced polymer composites. Int J Adv Manuf Technol 2016; 82: 1517–25, doi: 10.1007/s00170-015-7479-2